

1 Evidence Of Protein Collective Motions On The
2 Picosecond Time Scale

3 *Yunfen He¹, Jing-Yin Chen², Joseph R. Knab³, Wenjun Zheng¹, Andrea G. Markelz^{1*}*

4 ¹University at Buffalo, the State University of New York, ²Institute for Shock Physics,
5 Washington State University, ³Delft University of Technology

6

1 **Abstract**

2 We investigate the presence of structural collective motions on a picosecond time scale for the
3 heme protein, cytochrome c, as a function of oxidation and hydration, using terahertz (THz)
4 time-domain spectroscopy and molecular dynamics simulations. The THz response dramatically
5 increases with oxidation, with the largest increase for lowest hydrations and highest frequencies.
6 For both oxidation states the THz response rapidly increases with hydration saturating above
7 ~25% (g H₂O/g protein). Quasi-harmonic vibrational modes and dipole-dipole correlation
8 functions are calculated from molecular dynamics trajectories. The collective mode density of
9 states alone reproduces the measured hydration dependence providing strong evidence of the
10 existence of these motions. The large oxidation dependence is reproduced only by the dipole-
11 dipole correlation function, indicating the contrast arises from diffusive motions consistent with
12 structural changes occurring in the vicinity of a buried internal water molecule.

13

14 **Introduction**

15 Protein function relies on structural dynamics, with time scales ranging from picoseconds to
16 beyond seconds. The transitions to the different configurations involved in function are routinely
17 reproduced by trajectories involving only the first few structural collective vibrational modes,
18 suggesting the importance of these modes in understanding and tailoring of protein interactions.
19 However, there is some debate as to whether large scale structural collective motions exist and if
20 instead dynamics are entirely directed Brownian motion. Such uncorrelated diffusive motion
21 would need to serendipitously access the proper configuration for protein-protein or protein-
22 ligand binding. Concerted motions could explain the observed high physiological on-rates and

[Insert Running title of <72 characters]

1 affinities ¹⁻⁴. Recent neutron spin echo and X-ray inelastic scattering have verified that collective
2 motions do occur ^{5,6}, however these challenging measurements did not address the influence of
3 these modes on function. The nature of these measurements limits their broad application for
4 protein engineering. The question of coupling of large scale motion is critical in the quest for
5 tailoring allosteric interactions.

6 Computational studies of collective motions include normal modes, quasiharmonic modes and
7 course grain modes. An intuitive example of large-scale collective motion is the hinging motion
8 of lysozyme. The hinge motion is immediately apparent as the upper and lower portions of the
9 protein clamp down upon the substrate resulting in more effective cleavage. However one can
10 also visualize the molecule without substrate and the hinge continuously oscillating. This motion
11 was first calculated over 20 years ago by Karplus and Brooks using normal mode analysis for
12 lysozyme, with a hinge bending resonant frequency of $3.6 \text{ cm}^{-1} = 0.108 \text{ THz}$ ⁷. While there is
13 some skepticism if these harmonic motions occur in vivo the calculated modes lead to root mean
14 squared displacements in good agreement with experimental results ^{8,9}. The calculated time
15 scales for these correlated motions can be from the ps to ns.

16 To fully characterize these motions requires an experimental tool which can both resolve
17 energy and momentum transfer in the picosecond range. Inelastic neutron scattering (INS) is
18 such a technique, however its application is limited since it is not a table top instrument and
19 requires large samples (~100 mg) and deuteration. Another relevant spectral technique is
20 terahertz time domain spectroscopy (THz TDS). Previously we and others have used terahertz
21 time domain spectroscopy to measure the dielectric function of protein samples. The dielectric
22 response has contributions from vibrational and diffusive motions in the protein and adjacent
23 solvent:

[Insert Running title of <72 characters]

$$\varepsilon(\omega) = \varepsilon_o + \int \frac{f(\omega')g(\omega')}{(\omega'^2 - \omega^2) + i\gamma(\omega')\omega} d\omega' + \varepsilon_r \int_0^\infty \frac{h(\tau)d\tau}{1 + i\omega\tau} \quad (1)$$

where ε_o is the DC dielectric constant. The second term on the right hand side contains the vibrational density of states (VDOS) $g(\omega)$, oscillator strength $f(\omega)$ and damping coefficient $\gamma(\omega)$. The third term is the relaxational response, assuming Debye relaxation for a distribution of relaxation times $h(\tau)$. Typically, what is measured is the absorption coefficient $\alpha(\omega)$ and the refractive index $n(\omega)$. Relating these measured quantities to the vibrational and relaxational response, one obtains:

$$\alpha_{vib}(\omega) = \int \frac{g(\omega')f(\omega')\omega\gamma(\omega')}{(\omega'^2 - \omega^2)^2 + \gamma(\omega')^2\omega^2} d\omega' \quad \text{and} \quad \alpha_{relax}(\omega)n_{relax}(\omega) = \int \frac{1}{c} \frac{h(\tau)\tau\omega^2}{1 - \tau^2\omega^2} d\tau \quad (2)$$

where $\alpha_{vib}(\omega)$ is the absorption coefficient which arises from the vibrational motions and $\alpha_{relax}(\omega)n_{relax}(\omega)$ is the product of the absorption coefficient and refractive index arising from the relaxational response. The relaxational response is always a broad absorbance. For small systems (5-20 atoms), the frequency dependence of the vibrational and relaxational responses are distinct, with the vibrational resonances widely spaced and relatively narrow. For large macromolecules, the collective vibrational modes become dense and individual modes begin to overlap. The spectrum becomes sufficiently dense that it is difficult to distinguish the structural vibrational response from localized side chain relaxational rotations¹⁰. Such a distinction is important for applications such as allosteric inhibitor design, where the binding of the inhibitor is constructed to interfere with the structural motions necessary for function¹¹. Our ability to characterize global structural motions distinct from local diffusive ones is challenged by the

[Insert Running title of <72 characters]

1 similarity in the relaxational and vibrational response for large macromolecules. However the
2 manner in which these different types of motions change with environment or functional state
3 can be distinct. To test for the presence and contribution of picosecond collective vibrational
4 modes, we compare systematic measurements of cytochrome c (CytC) as a function of hydration
5 and oxidation with the calculated response from the collective vibrational motions and the
6 dipole-dipole correlation function which includes relaxational response. We find collective
7 vibrational motions account for the hydration dependence observed in the THz dielectric
8 response. However, the frequency dependence appears to be dominated by the relaxational
9 motions of water and side chains. Furthermore the large oxidation dependent dielectric response
10 observed experimentally is only reproduced when relaxational motions are included.

11 CytC is a protein of increasing interest as its multiple functions become revealed. The
12 primary role of CytC is to participate in the metabolism process in the mitochondria through the
13 transfer of an electron from cytochrome c reductase to cytochrome c oxidase, both embedded in
14 the inner mitochondrial membrane. Recently, it has become clear that CytC plays an important
15 role in apoptosis, both within the mitochondria and during its release into the cytosol ¹².
16 Furthermore, CytC is an excellent model heme protein to consider fundamental questions of
17 protein dynamics, as it is sufficiently small for systematic comparisons to theoretical modeling.

18 The physiochemical properties of CytC can be explained in terms of the differences in the
19 dynamic behavior of the two redox states. Eden and co-workers proposed that the oxidized form
20 of CytC is more flexible than the reduced form ¹³, based on an estimated 40% increase in the
21 apparent compressibility of CytC upon oxidation. X-ray diffraction measurements appeared to
22 give some support to higher flexibility in the ferri state, as the atomic mean squared displacement
23 (msd) as measured by the Debye Waller factor increases for ferri over ferro ¹⁴. The motions

[Insert Running title of <72 characters]

1 contributing to msd can be both collective as in structural vibrational modes and local as in side
2 chain librations. A quantitative relationship can be drawn between the collective modes and the
3 structural flexibility using the frequency dependence of the vibrational density of states (VDOS).
4 Low frequency modes below $k_B T$ are thermally occupied and these motions will contribute to the
5 msd, whereas high frequency modes with energies on the order of $k_B T$ or higher have lower
6 occupation and have a smaller contribution to the msd. THz-TDS was previously used to
7 investigate if the implied changes in the VDOS occurs with the CytC flexibility change with
8 oxidation ¹⁵. A large increase in the THz dielectric response was observed with oxidation
9 consistent with an increase in the low frequency VDOS and a higher flexibility. A number of
10 observations since those studies have suggested caution when directly relating the dielectric
11 response to the VDOS. These include the exploration of the role of local relaxational motions in
12 the THz dielectric response in hydration measurements on lysozyme ¹⁶; nuclear vibrational
13 resonance spectroscopy (NRVS) measurements showing a very slight increase in the VDOS for
14 the modes coupled to the heme Fe with oxidation of CytC ¹⁷; and the report of a large
15 enhancement in the dielectric response for water immediately adjacent to the protein over that of
16 bulk water ¹⁸. This last point is critical in that if the equilibrium water content is dependent on
17 oxidation state, the THz contrast observed may arise from the different water contributions and
18 not from a density of states change. It is therefore important that the comparison between
19 oxidation states be made at equivalent water content.

20 More importantly the systematic hydration and oxidation dependence data allows us to test the
21 degree structural vibrational modes contribute to the terahertz response and to determine the
22 origin of the oxidation dependence by comparison with molecular dynamics (MD) simulations.
23 We present two simulation approaches, both using calculated molecular trajectories: harmonic

[Insert Running title of <72 characters]

1 vibrational response based on quasiharmonic analysis; and the full response as determined by the
2 power spectrum of the dipole-dipole correlation function. Quasiharmonic analysis is also
3 referred to as principle component analysis (PCA). PCA is essentially a harmonic analysis
4 allowing for changes in the effective force constants at finite temperature. In this method, the
5 MD simulation is utilized to obtain effective modes of vibration from the atomic fluctuations
6 about an average structure. These modes include the anharmonic effects neglected in a normal
7 mode calculation¹⁹. PCA introduces temperature dependent anharmonicity, but still calculates
8 the harmonic vibrational modes of the system as well as the dipole derivative for each mode,
9 which is used to calculate the absorption coefficient. This analysis does not capture diffusive
10 motion such as librational motion of side chains and individual rotational motion of solvent
11 molecules. To capture the full dielectric response involving all motions one must use the
12 complete trajectory calculated from the full potential. The dipole-dipole correlation function is
13 calculated from the MD trajectories and then the Fourier transform of the correlation function
14 reveals the frequency dependent absorption coefficient. We perform both types of calculations
15 as a function of hydration and oxidation state and compare with the measured results.

16 We find the measured hydration dependence of the picosecond dynamics for both oxidation
17 states of CytC deviates from the typical rapid increase at 30 % wt, and that the VDOS calculated
18 using PCA reproduces the observed hydration dependence. This ability to reproduce the
19 measured hydration dependence with the quasiharmonic modes indicates the presence of
20 collective modes at THz frequencies. However PCA does not reproduce the observed oxidation
21 or frequency dependence. We find that the calculated dielectric response from the full dipole-
22 dipole correlation function which includes diffusive motions does reproduce the oxidation and
23 frequency dependence. We propose that the THz dielectric response is dominated by the

[Insert Running title of <72 characters]

1 anharmonic motions such as surface side chain rotational motions or possibly motion of an
2 internally bound water molecule.

3

4 **Experimental Details**

5

6 **Sample Preparation and Characterization:**

7 Preparation of oxidized and reduced CytC films measured in THz time domain spectroscopy is
8 described in a previous study¹⁵. Solutions were pipetted onto clean infrasil quartz substrates with
9 half the substrate left bare for referencing. The films were characterized by UV/Vis absorption
10 to verify the oxidation state (see supplementary material). The thickness of the dried films is
11 measured to both verify uniformity and to determine absolute absorption coefficients and
12 refractive indices. Film thicknesses were typically on the order of 100 nm with thickness
13 variation < 5% for a given film. See ref²⁰ for method of film thickness determination.

14

15 **Isotherm Determination:**

16 To compare the picosecond dielectric response of ferro and ferri samples at equivalent water
17 content we measured the isotherms for both oxidation states. The water content for a given
18 relative humidity often follows the B.E.T. thermal equation²¹:

$$19 \quad h(x) = \frac{ah_m x}{(1+x)[1+(a-1)x]} \quad (3)$$

20 where $h(x)$ is the water content as % wt, that is, g water/100 g protein; a is a parameter
21 representing the potential water absorption capacity of the protein; h_m is a parameter representing
22 the humidity for monolayer of water; and x is the relative pressure of the gas, namely, the
23 relative humidity. See supplementary material for method and results.

[Insert Running title of <72 characters]

1

2 THz TDS:

3 An N₂ purged terahertz time domain spectroscopy system (THz TDS) with bandwidth 5 cm⁻¹ -
4 86 cm⁻¹ is used to monitor the change in absorbance and index with oxidation states of CytC
5 films at different hydration. The THz radiation is generated by a Hertzian dipole antenna and
6 detected electro-optically.^{22,23} All measurements were performed at room temperature and under
7 hydration control. Substrates were mounted on a brass holder with two apertures for the
8 reference bare substrate and the CytC film. The plate is mounted in a closed hydration cell with
9 the relative humidity controlled by flushing the cell with a hydrated gas from a Licor dewpoint
10 generator. Nitrogen (air) was used as the flushing gas for the ferro (ferri) films. The closed
11 hydration cell is placed at the focus of the THz TDS system.

12 We measure the terahertz dielectric response of both oxidized and reduced CytC films as a
13 function of hydration. The time required for CytC films to reach hydration equilibrium is
14 determined by TGA (thermogravimetric analysis) and terahertz transmission and both found the
15 time for dehydration was ~ ½ hour and for hydration ~ 1 hour. To ensure equilibrium hydration
16 the samples were exposed to a given relative humidity in the hydration cell for at least one hour
17 for film dehydration and two hours for film hydration. The vertically mounted substrates limited
18 the highest hydration to below the film's threshold for flowing. For ferri (ferro) -CytC films, the
19 highest water content achieved was 75 % wt (57 % wt). A transmission measurement consists of
20 toggling between the sample and reference apertures. Absorption due to the gas phase water of
21 the humidity cell is removed by the reference which is in the same humidity cell as the sample.
22 The real part of the refractive index and the absorption coefficient are extracted from the
23 terahertz transmission data in the standard way²⁴.

[Insert Running title of <72 characters]

1

2 Molecular Dynamics Calculations:

3 We used Version 32 of CHARMM²⁵ with all-atom parameter set 22²⁶. The x-ray structure file
4 1hrc.pdb was used as the starting structure. Heme group partial charges for ferro and ferri states
5 are taken from reference²⁷. The heme group is patched to CytC though axial ligated bounds, Met
6 80 and His 18 and covalent bounds, Cys14 and Cys17. Different hydrations are simulated by
7 solvating the protein with a layer of water molecules with different thicknesses between 1.5 Å
8 and 7 Å by using the “SOAK” command in Insight II. The structures of the solvated proteins are
9 built in CHARMM by using TIP3 force field. The energy minimized structure was then used for
10 MD simulations.

11 MD simulations were carried out with an integration time step of 0.001 ps. The system was
12 heated to 300 K with a temperature increment of 100 K after each 1000 steps. Temperature
13 equilibration was followed by a constant temperature MD run. The trajectory is 1ns, starting with
14 399 ps equilibrium run, being followed by a 601ps production run. We find the water rapidly
15 moves to equilibrium positions with the water structure resembling X-ray measurements within
16 50 ps.

17 From the production run of the MD simulation the average structure of each protein was
18 determined separately using the corresponding 6001 frames and, superimposing each structure
19 onto the average structure, a quasiharmonic vibrational analysis was performed. This is done by
20 diagonalizing the whole covariance matrix for a given protein. The calculation output includes
21 the eigenvalues (mode frequency), the eigenvectors, and the dipole derivatives for each mode²⁸.

22 For mode frequency ν_k , the integrated intensity Γ_k has units of molar absorptivity and is
23 proportional to the absorption coefficient²⁹. We draw a distinction of Γ_k with the often

[Insert Running title of <72 characters]

1 calculated absorption intensity, A_k . A_k differs from Γ_k by a factor of ν_k and is not directly related
 2 to the derivation of the absorption coefficient from Fermi's Golden rule. The double harmonic
 3 approximation consists of modes calculated from a harmonic expansion of the potential and an
 4 approximation of the dipole moment inner product using the quadratic term in the Taylor
 5 expansion of the dipole. Γ_k can be obtained from the dipole derivatives calculated from the
 6 quasiharmonic analysis using³⁰:

$$7 \quad \Gamma_k = \frac{N_0 \pi^2}{3c^2 \epsilon_0 \omega_k} \left(\frac{\partial p}{\partial Q_k} \right)^2 \quad (4)$$

8 where ϵ_0 is the permittivity of vacuum, and N_0 is the Avogadro number and the magnitude of
 9 the dipole derivative

10 The net calculated absorption coefficient is proportional to the sum of Lorentzian oscillators
 11 with relaxation rates γ_k such that we define our quasi harmonic calculated absorption coefficient
 12 as

$$13 \quad \alpha_{QH}(\omega) = \sum_k \frac{1}{\pi} \frac{\Gamma_k \gamma^2}{(\omega - \omega_k)^2 + \gamma^2}. \quad (5)$$

14 γ is set to 4 cm^{-1} in agreement with the FWHM observed for THz vibrational resonances
 15 for molecular crystals.

16 The absorption coefficient per unit length $\alpha(\omega)$ and the refractive index $n(\omega)$ are related to the
 17 imaginary part of the dielectric constant $\epsilon''(\omega)$ by $\alpha(\omega)n(\omega) = (\omega/c) \epsilon''(\omega)$. Within linear-
 18 response theory, $\alpha(\omega) \nu(\omega)$ is given by the power spectrum of the time-correlation function of
 19 the total dipole operator³¹:

$$20 \quad \alpha(\omega)n(\omega) = \frac{2\pi\omega^2 \beta}{3cV} \int_{-\infty}^{\infty} dt e^{-i\omega t} \langle M(0)M(t) \rangle \quad (6)$$

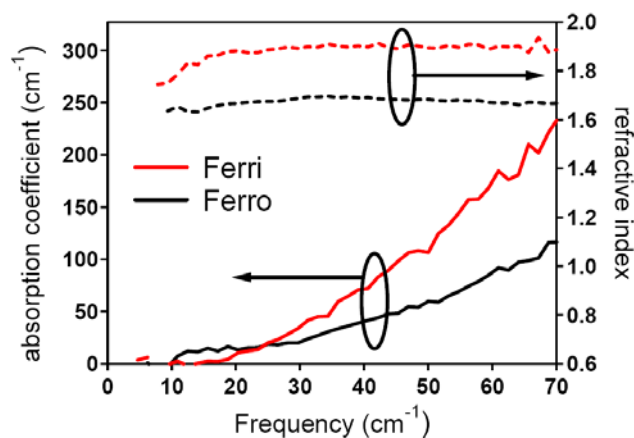
[Insert Running title of <72 characters]

1 Where M is the total dipole moment of the system, V is the volume of the system, and where
 2 $\beta = (k_B T)^{-1}$ is the inverse temperature. We calculate the time dependence of the total dipole
 3 moment $M(t)$ for the trajectory assuming constant partial charges for all atoms during the entire
 4 trajectory.

5

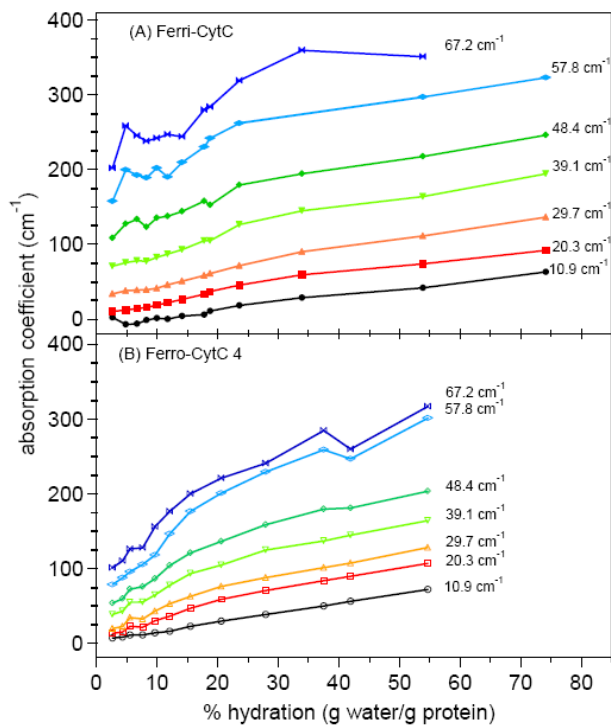
6 Results

7 In Figure 1, we show the measured frequency dependence of the THz absorption coefficient.
 8 The THz absorption of the ferri-CytC and ferro-CytC films increases monotonically with
 9 frequency. There are no distinct resonances observed in \square , however there is an obvious
 10 increase with oxidation. The refractive index of CytC films is nearly frequency independent up
 11 to 85 cm^{-1} and also has a large increase with oxidation ($n_{\text{ferro}} = 1.65$ to $n_{\text{ferri}} = 1.80$ for 3% h).



12

13 Fig. 1.



1

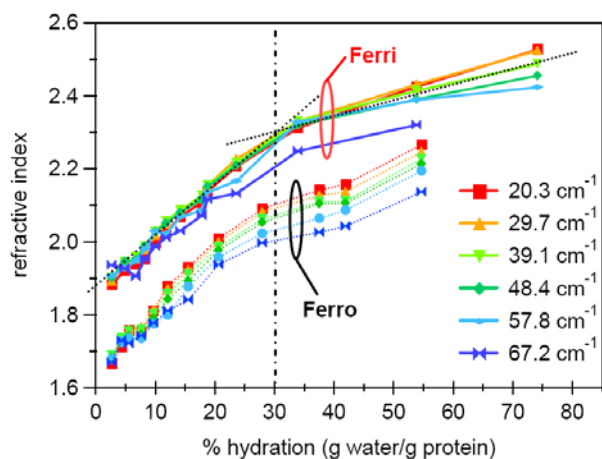
2 Fig. 2

3 We compare the absorption coefficients of ferri-CytC and ferro-CytC films as a function of
 4 water content in Figure 2. The absorption coefficient rapidly increases with hydration with the
 5 rate of increase abruptly decreasing at a cross over point $\sim 20\text{-}25\%$ wt. This cross over behavior
 6 from a rapid increase with hydration to a saturation behavior for both oxidation states is readily
 7 apparent in the refractive index data in Figure 3.

8 Comparing the response at equivalent water content we see in Figure 2 and 3, an obvious
 9 oxidation dependence of the picosecond response as was reported earlier. The dependence is
 10 most dramatic for the index measurements, where the ferri state values are consistently larger for
 11 all hydrations and frequencies. While the absorption coefficient does increase in the ferri state at
 12 higher frequencies and lower hydrations, this contrast decreases with increasing hydration and at
 13 lower frequencies. This oxidation dependence is consistent with Takano and Dickerson's B-

[Insert Running title of <72 characters]

1 factors where the average B-factor was found to increase from 18.7 in the ferro state, to 22.7 in
2 the ferri state¹⁴.

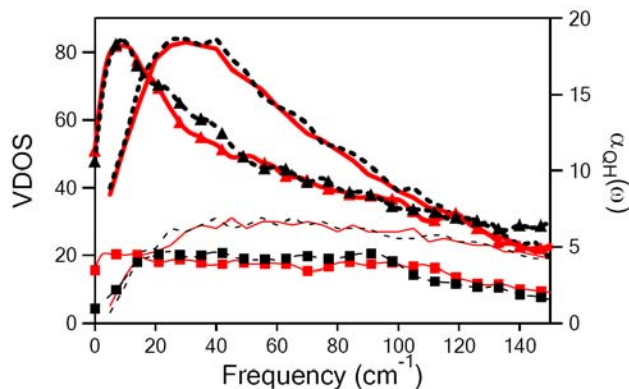


3

4 Fig. 3

5 We compare the measured response to the calculated response for only collective modes and
6 for the full response including local relaxational motions. In addition to PCA calculations
7 presented here, we performed the simpler normal mode analysis where the force constants are
8 extracted from the curvature of the potential at the minimized energy. We found little agreement
9 between the calculated normal modes and the measured frequency, hydration or oxidation
10 dependence indicating that normal mode analysis is inadequate for accurately describing the
11 dynamics at room temperature.

[Insert Running title of <72 characters]



1

2 Fig. 4

3 We first examine the frequency and oxidation dependence calculated using PCA. The

4 vibrational density of states (VDOS) and absorptivity for oxidized and reduced CytC are shown

5 in Figure 4. The VDOS increases with frequency reaching a peak at $\sim 30 \text{ cm}^{-1}$ and then

6 decreases. As the hydration increases, the number of quasiharmonic modes for oxidized and

7 reduced CytC also increases and the peak in the VDOS red shifts. This frequency dependence

8 does not resemble the measured dielectric response seen in Figure 1. Similarly there is no

9 apparent oxidation dependence in the VDOS. The absorptivity is calculated from the dipole

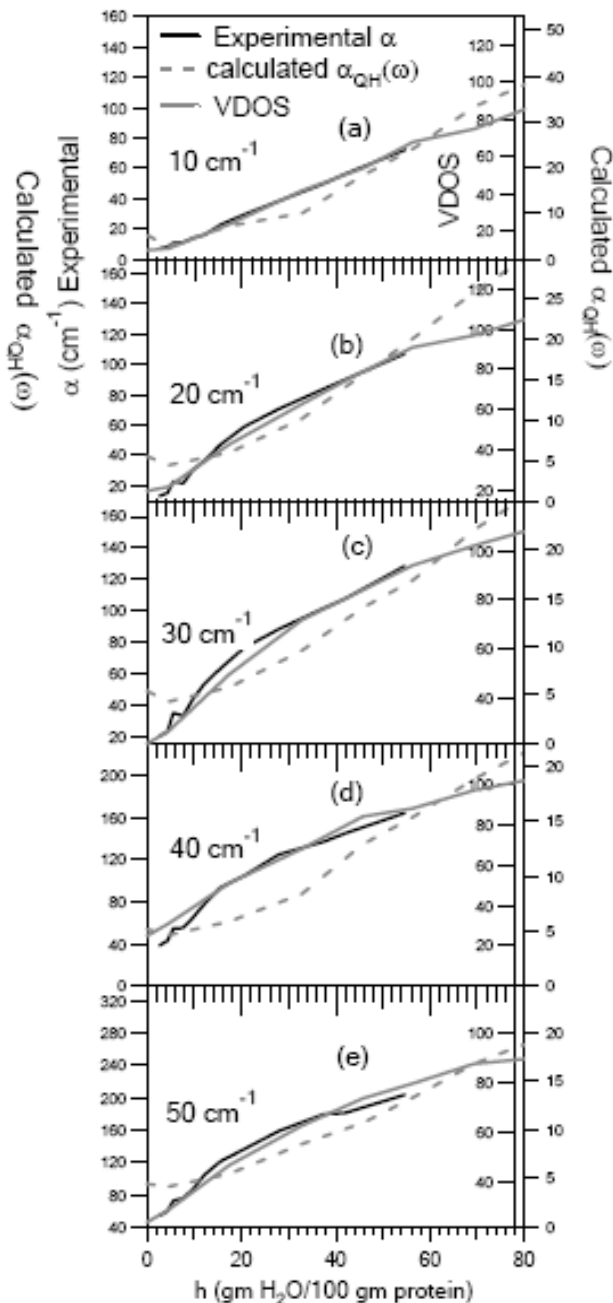
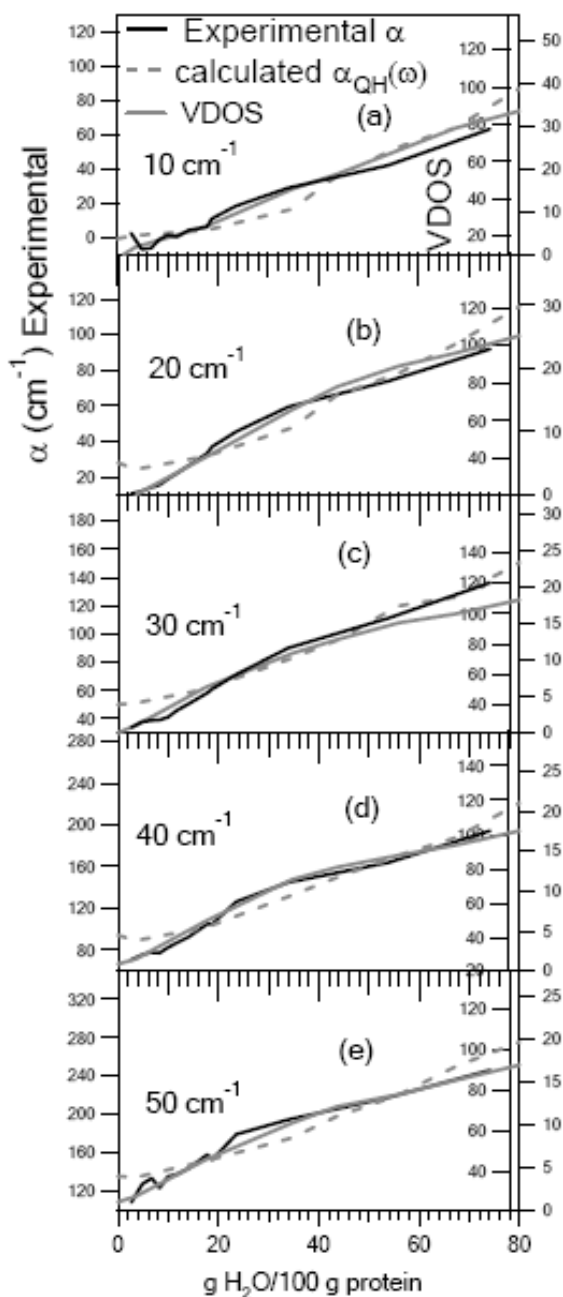
10 derivative of the mode. It is assumed the partial charges of the individual atoms remain constant

11 as the atoms move along the eigenvector, which is a problematic but common assumption.

12 Again neither the frequency or oxidation dependence of the calculated absorptivity from the

13 collective modes resembles the measured response.

[Insert Running title of <72 characters]



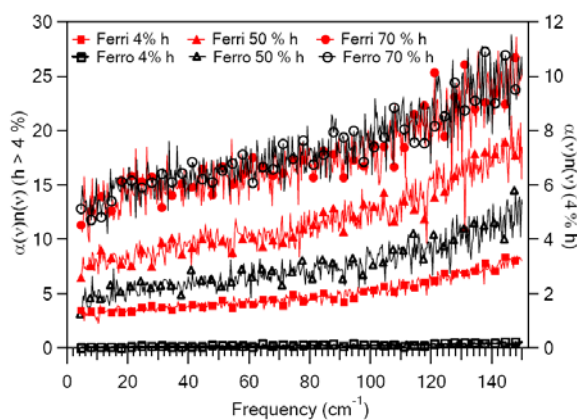
1

2 Fig. 5

Fig. 6

3 Figures 5 (6) shows a comparison of the hydration dependence of the measured absorption
 4 coefficient, the calculated VDOS and the calculated absorption coefficient for several
 5 representative frequencies for ferri (ferro) CytC. The observed hydration dependence for
 6 cytochrome c departs from the expected hydration dependence of protein dielectric response as
 [Insert Running title of <72 characters]

1 characterized over a broad frequency range up to 10 GHz 40 years ago³². There, for the proteins
 2 studied, the dielectric response increases slightly with hydration up to 30% wt then increases
 3 rapidly above this hydration. The rapid increase at 30 % wt is associated with anharmonic
 4 motions accessible with the increased plasticity with hydration³³⁻³⁶. This departure for the
 5 hydration dependence of CytC response provides a test for the MD simulations. We see in Figs.
 6 5 and 6 the collective mode VDOS reproduces the hydration dependence well for both oxidation
 7 states and over the entire frequency range. This agreement suggests A) the presence of structural
 8 vibrational modes contributing to the dielectric signal and B) these modes are responsible for the
 9 observed hydration dependence. The hydration dependence of the calculated absorption
 10 coefficient does not reproduce the measurements as well. It is possible that this is in part due to
 11 the assumption of constant partial charges in the dipole derivative calculations.



12

13 Fig. 7

14 It is clear that the collective modes do not give rise to the oxidation sensitivity of the THz
 15 response. The PCA calculations for this frequency range account only extended oscillatory
 16 motions. The Fourier transform of the dipole-dipole correlation gives the product of the
 17 frequency dependent absorption coefficient and the refractive index, $\alpha(\omega)\nu(\omega)$ which includes all
 18 motions contributing to the response, including local relaxational motions of water and surface
 [Insert Running title of <72 characters]

1 side chains. As shown earlier, the measured refractive index has little frequency dependence so
2 we directly compare the calculated $\alpha(\omega)\nu(\omega)$ with the measured $\alpha(\omega)$. In Figure 7 we show the
3 frequency dependence for $\alpha(\omega)\nu(\omega)$ several hydrations. The frequency dependence now
4 resembles the measured absorption coefficient and we see that at low hydration there is a strong
5 contrast between oxidized and reduced cytochrome c. As the hydration increases this difference
6 decreases. At the highest hydration levels one cannot distinguish between the two oxidation
7 states.

8

9 **Discussion**

10 The hydration dependent collective mode calculations indicate their contribution to the
11 dielectric response. As seen in Figure 4, the collective modes do not reproduce the frequency
12 and oxidation dependencies. While the modes at increasingly higher frequencies progressively
13 more localized, the motions even up to 300 cm^{-1} are extended beyond individual residues (see
14 supplemental material). The quasiharmonic VDOS never captures the low frequency diffusive
15 motions of surface side chains. The residence times for these motions were calculated with
16 typical times $\sim 2\text{-}10\text{ ps}$ ³⁷. These motions have been discussed by Sokolov and others when
17 analyzing the anharmonicity in the neutron temperature dependence³⁸ and will be present in the
18 calculated full trajectory. That the observed oxidation state dependence is not reproduced by any
19 of the harmonic analysis, but is reproduced by the dipole-dipole correlation indicates that the
20 oxidation dependence arises from relaxational motions. We suggest that the internal bound
21 water dynamics are influenced by the local electrostatics and it is these motions that give rise to
22 the oxidation dependence seen in the THz response. At low hydrations these few internally
23 bound waters provide a large contribution to the overall signal and therefore an oxidation

[Insert Running title of <72 characters]

1 dependence is observed. At higher hydrations the surface water, mobile surface side chains and
2 the vibrational modes begin to dominate the signal, and the internal water has little net
3 contribution, so the oxidation dependence is no longer significant at the higher hydrations.

4 We note the contrast seen in the THz measurements is not seen by another important protein
5 dynamics characterization technique nuclear resonant vibrational spectroscopy (NRVS)³⁹. An
6 extensive NRVS study found only a very slight increase with oxidation for CytC^{17,40}.
7 Accompanying this, MSD simulations for the heme group and backbone had no discernible
8 oxidation dependence. These calculations did not include the diffusive water or side chain
9 motion. The oxidation dependence arising from internal water diffusive motion could explain
10 why little oxidation dependence is seen by NRVS, as there the samples were fully hydrated and
11 the motions observed are vibrational modes coupled to the heme Fe.

12

13 **Conclusion**

14 To conclude, terahertz spectroscopy is sensitive to protein environment and functional state.
15 Structural collective modes as calculated by PCA reproduce the measured hydration dependence
16 of absorption coefficient, demonstrating their contribution to the picosecond response. The
17 oxidation dependence of the picosecond response is only reproduced by analysis of the complete
18 trajectory, demonstrating that it is manifest only in the diffusive motions of either the side chains
19 or the internal water. The evidence of structural collective modes in these smaller molecular
20 weight proteins is consistent with recent results using neutron spin echo measurements (NSE) on
21 somewhat more massive proteins^{6,41}. The terahertz spectroscopy approach may provide a
22 critical complementary technique to NSE for collective modes on shorter time scales.

23

[Insert Running title of <72 characters]

1 Acknowledgements

2 This work was supported by ARO grant DAAD 19-02-1-0271, ACS grant PRF 39554-AC6,
3 NSF CAREER grant PHY-0349256, NSF REU grant DMR-0243833 and NSF IGERT grant
4 DGE0114330.

6 References

- 7 (1) Goodey, N. M.; Benkovic, S. J. *Nature Chemical Biology* **2008**, *4*, 474-82.
- 8 (2) Hammes-Schiffer, S.; Benkovic, S. J. *Annu. Rev. Biochem.* **2006**, *75*, 519-41.
- 9 (3) Lange, O. F.; Lakomek, N.-A.; Farès, C.; Schröder, G. F.; Walter, K. F. A.;
10 Becker, S.; Meiler, J.; Grubmüller, H.; Griesinger, C.; Groot, B. L. d. *Science* **2008**, *340*, 1471-
11 75.
- 12 (4) Jarymowycz, V. A.; Stone, M. J. *Chem. Rev.* **2006**, *106*, 1624-1671.
- 13 (5) Liu, D.; Chu, X.-q.; Lagi, M.; Zhang, Y.; Fratini, E.; Baglioni, P.; Alatas, A.;
14 Said, A.; Alp, E.; Chen, S.-H. *Phys. Rev. Lett.* **2008**, *101*, 135501.
- 15 (6) Biehl, R.; Hoffmann, B.; Monkenbusch, M.; Falus, P.; Pre'ost, S.; Merkel, R.;
16 Richter, D. *Phys. Rev. Lett.* **2008**, *101*, 138102.
- 17 (7) Brooks, B.; Karplus, M. *Proceedings of the National Academy of Sciences of the*
18 *United States of America* **1985**, *82*, 4995-4999.
- 19 (8) Teeter, M. M.; Case, D. A. *J. Phys. Chem.* **1990**, *94*, 8091-97.
- 20 (9) Zoete, V.; Michielin, O.; Karplus, M. *J. Mol. Biol.* **2002**, *315*, 21-52.

[Insert Running title of <72 characters]

- 1 (10) Markelz, A. G. *IEEE J. Sel. Topics in Quantum Electronics* **2008**, *14*, 180-190.
- 2 (11) Kern, D.; Zuiderweg, E. R. *Current Opinion in Structural Biology* **2003**, *13*, 748–
3 757.
- 4 (12) Kagan, V. E.; Bayir, A.; Bayir, H.; Stoyanovsky, D.; Borisenko, G. G.; Tyurina,
5 Y. Y.; Wipf, P.; Atkinson, J.; Greenberger, J. S.; Chapkin, R. S.; Belikova, N. A. *Mol. Nutr.*
6 *Food Res.* **2009**, *53*, 104-114.
- 7 (13) Eden, D. M., James B.; Rosa, Joseph J.; Richards, Frederic M. *Proceedings of the*
8 *National Academy of Sciences of the United States of America* **1982**, *79*, 815-819.
- 9 (14) Takano, T.; Dickerson, R. E. *Proceedings of the National Academy of Sciences of*
10 *the United States of America* **1980**, *77*, 6371-6375.
- 11 (15) Chen, J.-Y.; Knab, J. R.; Cerne, J.; Markelz, A. G. *Phys. Rev. E. Rapid* **2005**, *72*,
12 040901.
- 13 (16) Knab, J. R.; Chen, J. Y.; He, Y.; Markelz, A. G. *Proc. of the IEEE* **2007**, *95*,
14 1605-10.
- 15 (17) Leu, B. M.; Ching, T. H.; Zhao, J.; Sturhahn, W.; Alp, E. E.; Sage, J. T. *J. Phys.*
16 *Chem. B* **2009**, *113*, 2193–2200.
- 17 (18) Ebbinghaus, S.; Kim, S. J.; Heyden, M.; Yu, X.; Heugen, U.; Gruebele, M.;
18 Leitner, D. M.; Havenith, M. *Proc. Natl. Acad. Sci. U.S.A.* **2007**, *104*, 20749–20752.
- 19 (19) Balog, E.; Becker, T.; Oettl, M.; Lechner, R.; Daniel, R.; Finney, J.; Smith, J. C.
20 *Phys. Rev. Lett.* **2004**, *93*, 28103.

[Insert Running title of <72 characters]

- 1 (20) Whitmire, S. E.; Wolpert, D.; Markelz, A. G.; Hillebrecht, J. R.; Galan, J.; Birge,
2 R. R. *Biophys. J.* **2003**, *85*, 1269-1277.
- 3 (21) Gascoyne, P. R. C.; Pethig, R. *J. Chem. Soc. Faraday Trans.* **1977**, *73*, 171-180.
- 4 (22) Grischkowsky, D.; Katzenellenbogen, N. In *OSA Proceedings on picosecond*
5 *electronics and optoelectronics*; Sollner, T. C. L., Shah, J., Eds.; OSA: Washington, DC, 1991;
6 Vol. 9.
- 7 (23) Jiang, Z.; Zhang, X.-C. *IEEE TRANSACTIONS ON MICROWAVE THEORY AND*
8 *TECHNIQUES* **1999**, *47*, 2644-2650.
- 9 (24) Knab, J.; Chen, J.-Y.; Markelz, A. *Biophys. J.* **2006**, *90*, 2576-2581.
- 10 (25) Brooks, B. R.; Bruccoleri, R. E.; Olafson, B. D.; States, D. J.; Swaminathan, S.;
11 Karplus, M. *J. Comput. Chem.* **1983**, *4*, 187-217.
- 12 (26) MacKerell, A. D., Jr.; Bashford, D.; Bellott, M.; Dunbrack, R. L.; Evanseck, J. D.;
13 Field, M. J.; Fischer, S.; Gao, J.; Guo, H.; Ha, S.; Joseph-McCarthy, D.; Kuchnir, L.; Kuczera,
14 K.; Lau, F. T. K.; Mattos, C.; Michnick, S.; Ngo, T.; Nguyen, D. T.; Prodhom, B.; Reiher, W. E.,
15 III; Roux, B.; Schlenkrich, M.; Smith, J. C.; Stote, R.; Straub, J.; Watanabe, M.; Wiorcikiewicz-
16 Kuczera, J.; Yin, D.; Karplus, M. *J. Phys. Chem. B* **1998**, *102*, 3586-3616.
- 17 (27) Autenrieth, F.; Tajkhorshid, E.; Baudry, J.; Luthey-Schulten, Z. *Journal of*
18 *Computational Chemistry* **2004**, *25*, 1613-1622.
- 19 (28) Levy, R. M.; Rojas, O. d. l. L.; Friesner, R. A. *J. Phys. Chem.* **1984**, *88*, 4233-
20 4238.

[Insert Running title of <72 characters]

- 1 (29) Person, W. B.; Zerbi, G. *Vibrational Intensities in Infrared and Raman*
2 *Spectroscopy*; Elsevier Scientific Publishing, 1982.
- 3 (30) Galabov, B. S.; Dudev, T. *Vibrational Intensities*; Elsevier Science: Amsterdam,
4 1996.
- 5 (31) McQuarrie, D. A.; First ed.; University Science Books: Sausalito, CA, 2000.
- 6 (32) Harvey, S. C.; Hoeskstra, P. *J. Phys. Chem.* **1972**, *76*, 2987-2994.
- 7 (33) Pethig, R. *Dielectric and electronic properties of biological materials*; First ed.;
8 Wiley: New York, 1979.
- 9 (34) Bone, S.; Pethig, R. *Journal of Molecular Biology* **1982**, *157*, 571-575.
- 10 (35) Bone, S.; Pethig, R. *Journal of Molecular Biology* **1985**, *181*, 323-326.
- 11 (36) Rupley, J. A.; Careri, G. *Adv. Protein Chem.* **1991**, *41*, 37-172.
- 12 (37) Best, R. B.; Clarke, J.; Karplus, M. *J. Mol. Biol.* **2005**, *349*, 185-203.
- 13 (38) Roh, J. H.; Novikov, V. N.; Gregory, R. B.; Curtis, J. E.; Chowdhuri, Z.; Sokolov,
14 A. P. *Phys. Rev. Lett.* **2005**, *95*, 038101.
- 15 (39) Achterhold, K.; Keppler, C.; Ostermann, A.; Bu'rck, U. v.; Sturhahn, W.; Alp, E.
16 E.; Parak, F. G. *Phys. Rev. E* **2002**, *65*, 051916.
- 17 (40) Leu, B. M.; Zhang, Y.; Bu, L.; Straub, J. E.; Zhao, J.; Sturhahn, W.; Alp, E. E.;
18 Sage, J. T. *Biophysical Journal* **2008**, *95*, 5874-5889.

1 (41) Bu, Z.; Biehl, R.; Monkenbusch, M.; Richter, D.; Callaway, D. J. E. *Proc Natl*
2 *Acad Sci U S A.* **2005**, *102*, 17646–17651.

3
4

5 **Legends**

6 Figure 1. Frequency dependence of THz absorption coefficient and index. The THz absorption
7 coefficient and index are shown for Ferri-CytC film and a Ferro-CytC film at different
8 hydrations as a function of frequency.

9 Figure 2. Hydration dependence of THz absorption coefficients. THz absorption coefficients of
10 Ferri (A) and Ferro (B) CytC are shown for several representative frequencies as a function %
11 hydration. The data shows a rapid increase and then saturation of the response with hydration.

12 Figure 3. Hydration dependence of THz refractive indices. Refractive indices of Ferri (A) and
13 Ferro (B) CytC are shown for several representative frequencies as a function of % hydration.
14 Lines drawn as guide to the eye. The rapid turn over of the hydration dependence is nearly
15 frequency independent in contrast to the absorption coefficients shown in Figure 2.

16 Figure 4. Frequency and oxidation dependence of the calculated collective modes. The VDOS
17 and absorbtivity calculated from PCA is shown as a function of frequency for ferri (red solid
18 lines) and ferro (black dashed lines). The lines without markers are for the VDOS and the lines
19 with markers are for absorbtivity. Thick lines are for 50% h and thin lines for 4% h. Neither the
20 oxidation dependence nor the frequency dependence are the same as that observed.

21

[Insert Running title of <72 characters]

1 Figure 5. Comparison of the calculated structural collective mode to the measured hydration
2 dependence. The measured absorption coefficient, calculated quasiharmonic VDOS, and
3 calculated absorbance $\alpha_{QH}(\omega)$ for Ferri-CytC is shown as a function of hydration for several
4 representative frequencies. The calculated VDOS has good agreement with the measured
5 hydration dependence, suggesting the hydration dependence arises from these motions.

6

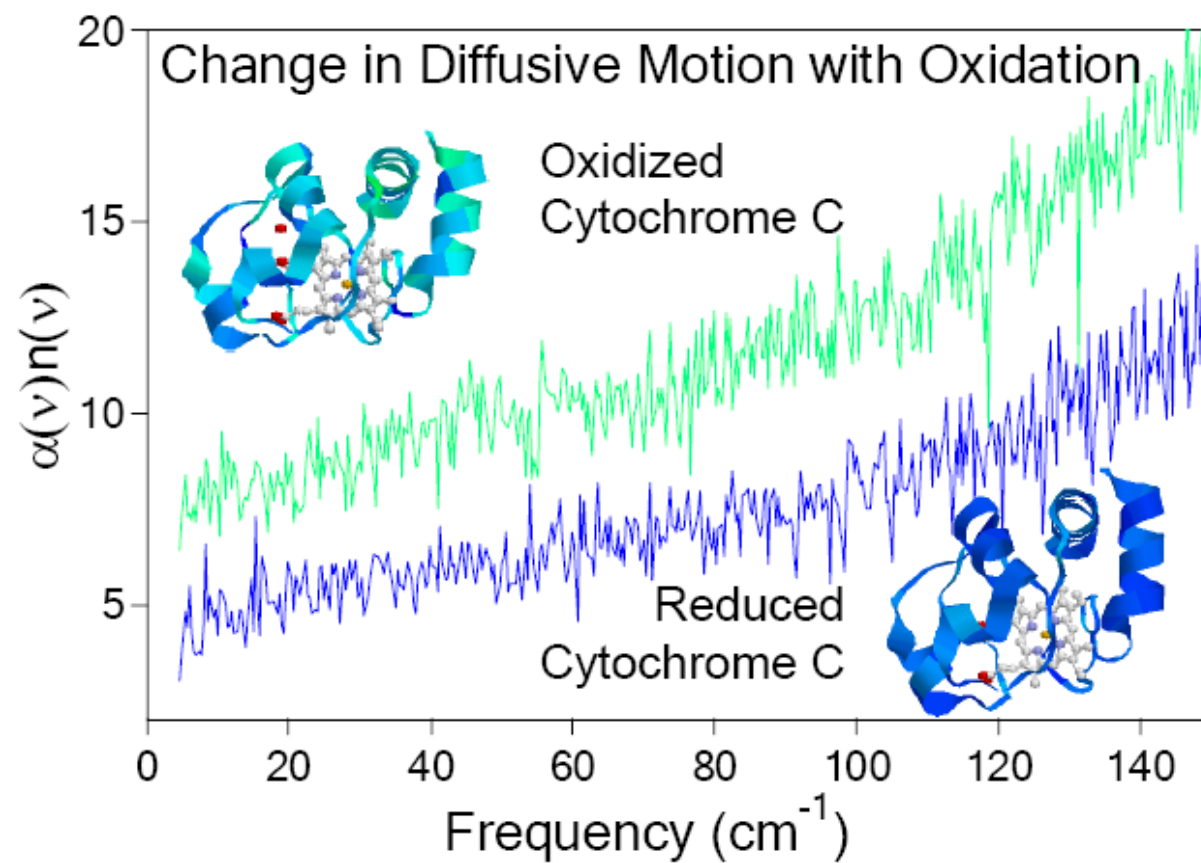
7 Figure 6. Comparison of the calculated structural collective mode to the measured hydration
8 dependence. The measured absorption coefficient, calculated quasiharmonic VDOS, and
9 calculated absorbance $\alpha_{QH}(\omega)$ for Ferro-CytC is shown as a function of hydration for several
10 representative frequencies. The calculated VDOS agrees well with the experimental results
11 similar to the ferri results in Figure 4. The agreement suggests the hydration dependence arises
12 from these motions.

13

14 Figure 7. The frequency dependent $\alpha(\omega)n(\omega)$ calculated from dipole-dipole correlation for
15 oxidized CytC (red, filled symbols) and reduced CytC (black, empty symbols) for several
16 hydration levels. The right axis corresponds to $h < 4\%$. The left axis corresponds to the
17 hydration $>46\%$. The 76 % h ferri and 78 % h ferro data are both offset by the same 5 units to
18 avoid overlap with the lower hydration data. At the lower hydration levels the ferro CytC
19 response is less than the ferri CytC. As the hydration increases, the difference with oxidation
20 decreases. The calculated response includes both local diffusive motions and long range
21 collective motions.

[Insert Running title of <72 characters]

1 Table of Contents Figure



2

[Insert Running title of <72 characters]